

Research article

Synthesis and characterization of CoFe_2O_4 /cellulose fiber nanocomposites

Ashwini Rayar¹, Naveen Chikkahanumajja Surendranatha²,
Honnenbagi Shivamurthy Onkarappa³, Pradeep Heregangur Keshavamurthysetty⁴,
Prasanna Gunderi Dhananjaya^{1*}

¹Department of Studies in Physics, Davangere University, Davangere, 577007 Karnataka, India

²Department of Physics, School of Engineering, Presidency University, Bengaluru, 560064 Karnataka, India

³Department of Chemistry, GM Institute of Technology, Davanagere, 577006 Karnataka, India

⁴Department of Pharmaceutics, GM Institute of Pharmaceutical Sciences and Research, Davanagere, 577006 Karnataka, India

Received 20 December 2023; accepted in revised form 19 February 2024

Abstract. Controlled development of novel materials fosters innovation in the electrical sector. The hybrid materials based on magnetic nanocellulose are intriguing since they have many uses in electronics, catalysis, medicine, and ecology. The study investigated the structure and morphology of hybrid nanomaterials made from nanocellulose and cobalt ferrite. The nanocellulose was prepared by TEMPO-oxidation and the cobalt ferrite was prepared by sol-gel auto-combustion method. Using X-ray diffraction (XRD) and Fourier-transform infrared spectroscopy (FTIR) techniques, it was determined how nanocellulose loading affected the crystal structure of the synthesized composite. To ascertain the variation in the component concentrations, scanning electron microscope (SEM) and energy-dispersive X-ray analysis (EDAX) are used. Composite with a higher concentration of nanocellulose fibers (NCF) show lesser particle size, and this may account for the smaller size of nanocellulose fibers, and attachment of nanocellulose nanofibers over the surface of porous cobalt ferrite (CF) found in SEM images.

Keywords: natural fiber, fibrous polymers, crystal structure, semicrystalline polymer, nanocellulose

1. Introduction

Metal nanoparticle-based magnetic ferrite nanocomposites are a topic of intense research due to their special applications in various fields, particularly nanobiotechnology [1, 2]. Additionally, these materials have drawn a lot of interest for use in biomedical applications, such as targeted drug delivery [3], immunoassays [4], magnetic contrast resonance imaging (MRI) [5, 6], bioseparation [7], and hyperthermia [8]. They can also be used for spintronics [9], the absorption medium for microwaves [10], humidity sensors [11], and many others. Controlling key characteristics of ferrite nanoparticles, such as acceptable

polarization losses, nanoparticle size distribution, and saturation magnetization, is crucial for these applications. Ferrite nanostructures have magnetic features that can be altered by substituting nonmagnetic metal cations and by changing the way they are prepared. Different ferrite nanostructures with particular particle sizes or compositions have been created over several decades. Mixed-metal ferrites have benefited from advanced synthetic processes such as cobalt ferrite (CoFe_2O_4) and manganese ferrite (MnFe_2O_4) [12]. Nanocellulose stands out among the numerous materials utilized as templates for synthesizing magnetic

*Corresponding author, e-mail: prasannagd@gmail.com

© BME-PT

nanoparticles because of its environmental biodegradability, high surface area, low density, superior mechanical capabilities, and ease of chemical modification [13]. By creating a nanofiber network during the formation/condensation of nanoparticles, the hydrogen bond between the hydroxyl groups on the cellulose surface plays a critical role in crystalline packing, enabling surface modifications that actively participate in the reaction.

In the coming generation of renewable nanomaterials for high-performance, environmentally friendly materials, nanocellulose is being considered [14]. Nanocellulose is a general term that describes different types of nano- and micro-sized cellulose particles, including (from largest to smallest) microfibrillated cellulose (MFC) [15], cellulose nanofibres (NCF) [16], and cellulose nanocrystals (CNC) [13] completely degrade a wide range of organic pollutants. Active sulfate and oxygen groups have been produced using metal ions (Co^{2+} , Cu^{2+} , Ce^{3+} , and Fe^{2+}), their metal oxides, and their metal-organic framework [17]. There is a variety of metal nanoparticles that can be used as dispersed phases in bio nanocomposites with cellulose. Inorganic nanoparticles have significantly advanced colloidal synthesis over the past few decades. Due to their distinct electrical, magnetic, optical, and antibacterial capabilities, colloidal metal nanoparticles have attracted much attention. An intense study has been done on their usage in composite materials as a result of their small size, huge specific surface area, and tunable physicochemical properties that differ significantly from the bulk analogs. Examples of studies on metal nanoparticles employed as fillers in cellulose nanocomposites are provided in this article. Although novel features result from the usage of metal nanoparticles and cellulose together, the applications of these materials depend on the type of nanoparticles present. Cobalt nanoparticles in cellulose have attracted attention because of their possible use in magnetic nanocomposites.

Surface atoms play a significant role in determining the characteristics of magnetic cobalt nanoparticles. Additionally, the material's response to a magnetic field depends on its size distribution, crystallinity, particle form, and nearby particles. As a result, the matrix—in this case, cellulose in which the nanoparticles are placed, significantly impacts both nanoparticle's magnetic characteristics and their distance from one another. The magnetic characteristics of

cobalt nanoparticles produced in a cellulose matrix and their shape and structure have been reported [18]. Amiralian *et al.* [19] described the hydrolysis synthesis method of nanocellulose and metallic ferrite compounds. The properties of the composites change with the variation in the concentration of nanocellulose fibers. They are utilized as a strong reagent to remove dye from the adsorbent. Oprea *et al.* [20] reported the composite of nanocellulose and metal oxides. Nanocellulose, when combined with metal oxides, show some properties that can be used as a substitute for antibacterial medicine. Korotcenkov [21] explained the utility of cobalt ferrite cellulose nanocomposite in gas sensing material. These materials pose high porosity, and a high surface-to-volume ratio of the porosity leads to higher gas permeability. A high surface-to-volume ratio makes them highly sensitive, which can provide speedy responses, allowing them to find applications in gas sensors. Thus, we are motivated to create cobalt ferrite (CF), nanocellulose fiber (NCF) composites and investigate their features by considering the numerous applications of nanocellulose and cobalt ferrite.

2. Materials and methods

AR grade ferric nitrate ($\text{Fe}(\text{NO}_3)_3 \cdot 9\text{H}_2\text{O}$) and cobalt nitrate ($\text{Co}(\text{NO}_2)_3 \cdot 6\text{H}_2\text{O}$), glycine ($\text{C}_2\text{H}_5\text{NO}_2$) was procured from S D Fine-Chem Ltd., Mumbai (India), nanocellulose fibers extracted from sugar cane bagasse. Distilled water was used throughout the experiments.

2.1. Synthesis of cobalt ferrite nanoparticles

CoFe_2O_4 (CF) was prepared by sol-gel auto-ignition method. The molar ratio of metal nitrates to glycine was 1:3. The precursor's ferric nitrate and cobalt nitrate is dissolved separately in distilled water. Then, 20.19 g of ferric nitrate was dissolved in 25 ml of distilled water corresponding to the 2 M solution by mass, and 7.28 g of cobalt ferrite was dissolved in 25 ml of distilled water corresponding to 1 M solution. These solutions are mixed thoroughly using a magnetic stirrer. 11.26 g of glycine is dissolved in 50 ml of distilled water, corresponding to a 3 M solution. The solution of ferric nitrate has a light brown color. The cobalt nitrate solutions are dissolved carefully to ensure the absence of precipitation with the help of a magnetic stirrer [22].

Cobalt nitrate was added to a solution of ferric nitrate drop by drop until the solution dissolves well. Fuel

glycine solution was added drop by drop. The solution was kept stirring and heated up to 70 °C temperature (Figure 1c). The pH of the solution was held to 7 by adding ammonium hydroxide. Once the solution reaches 70 °C, the solution was transferred to a container with a large surface area, where the container was preheated with the help of a heating mantle. After transferring the solution into the container, the solution was further heated to a higher temperature in the mantle, and heating the blackish solution will start thickening and reach a gel-like phase (Figure 1d). The thickening of the solution is due to the vaporization of water, CO₂, and NO₂ from the solution. With further heating of the thick gel, it will start boiling and gradually catch fire while burning the gel. Once the gel is captured, the fire gel converts to ash forms within a few seconds. The ash will be further heated to confirm the evaporation of any moisture. The ash will later be collected and ground well by using mortar. After grinding, the ash will take the form of a fine powder. This fine powder will be further calcined to 600 °C in the muffle furnace to eliminate impurities. This process is depicted in Figure 1.

2.2. Synthesis of nanocellulose

Lignocellulose material contains hemicellulose α -cellulose and lignin; nanocellulose was prepared using α -cellulose, and the pre-treatment is used to acquire a good quality of nanocellulose. The treatment of alkaline and hemicellulose removes lignin by the bleaching treatment [23].

2.2.1. Pre-treatment of lignocellulose material

Before pre-treatment, raw material is washed, dried, and sieved into smaller sizes, removing the non-cellulosic composition. Alkaline pre-treatment was

carried out in which fibers were immersed in a 5% NaOH solution at a specified temperature and time. The fibers break down to form finer ones, removing wax, hemicellulose, and pectin in the fiber. The end product was dispersed in 5% NaOH solution for 3 h under constant stirring, temperature up to 80–100 °C maintained and pH to neutral by washing the product [24].

It is followed by bleaching process which is used to remove hemicellulose and lignin in phenolic and chromophore groups; various bleaching agents were NaClO₃ and H₂O₂ under the acidic pH, and the alkaline treatment material was dispersed in the 5% of solution for NaCl₂ for 2–3 h and temperature 80–100 °C, The entire lignin was removed, the pulp is obtained and washed and filtered until it reaches the neutral pH and dried [24].

2.2.2. Extraction methods

Two methods can be used to extract nanocellulose: one is the chemical method, and another is the mechanical method. The chemical process includes acid hydrolysis, TEMPO oxidation and ionic liquid, and the automated process provides ultra-sonication [25, 26]. TEMPO oxidation method was employed for the extraction of nanocellulose as shown in Figure 2.

TEMPO oxidation method

TEMPO stands for 2,2,6,6-tetramethyl-1-piperidinyloxy, TEMPO oxidation was used to isolate nanocellulose fibers (NCFs). TEMPO is water soluble stable radical, 1 g of cellulose was dispersed in 100 ml of water. TEMPO was taken with 50 ml of water and added to cellulose solution, then 0.1 g of NaBr was added to cellulose solution, by adding 10% of NaCl, oxidation takes place by maintaining the pH 7. Adding NaOH, the solution is treated in

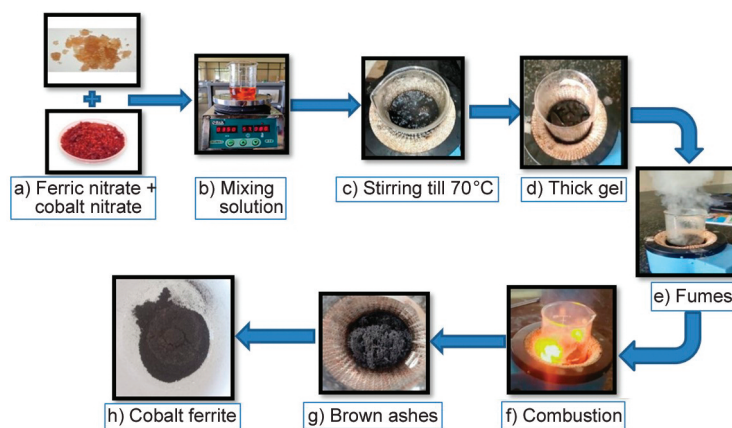


Figure 1. Schematic representation of synthesis of cobalt ferrite.

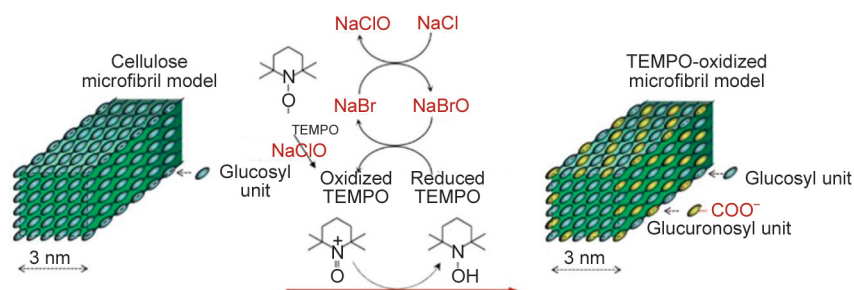


Figure 2. Schematic representation of the TEMPO-oxidation method [24].

ultrasonication to attain homogenization. The end product was washed and stored at 4 °C in a refrigerator. Cellulose nanofibers (NCF) contain many hydroxyl groups; the nanocellulose is obtained from mechanical treatment forms. Nano fibrillated cellulose, cellulose nanofibers have a large surface area. This method received 95% of the product [23, 27].

2.3. Synthesis of cobalt ferrite and nanocellulose fiber composite

The composites of nanocellulose fibers and cobalt ferrite are synthesized in two different proportions 50:50 and 75:25 by mass. The flowchart for the synthesis of cobalt ferrite and nanocellulose fibers composite is depicted in Figure 3. To synthesize a composite of ratio 50:50, 3 g of nanocellulose fibers are added to 100 ml of distilled water. The nanocellulose fibers itself, being in a gel-like form, get dissolved

in distilled water after continuously stirring the solution for about 15 min with the help of the magnetic stirrer. This forms a homogeneous solution of cellulose nanofibers. Then, 3 g of cobalt ferrite is added to 100 ml of the water and sonicated for around 30 min; this forms homogeneous solutions. Soon after the sonication of cobalt ferrite, the nanocellulose fiber solution is added dropwise to the sonicated cobalt ferrite solution and sonicated for 1 h. The obtained product is filtered, and the precipitate gets separated by water. The precipitate is collected and dried in a hot air oven at 70 °C for 3 h to eliminate the moisture and impurities [28]. Therefore, the composite of a 50:50 ratio was obtained.

Similarly, for synthesizing the composite of ratio 75:25 cobalt ferrite-nanocellulose fiber, 4.5 g of cobalt ferrite is sonicated in 100 ml of distilled water, and 1.5 g of cellulose nanofiber is dissolved in 100 ml of distilled water. The cellulose nanofibers solution is added to cobalt ferrite solution dropwise, which is sonicated for 3 h. After sonication, a clear precipitate is formed at the bottom, separated from the water. The solution is filtered using Whatman filter paper, and the precipitate composite gets separated. The separated residue will be dried in a hot air oven for 3 h, and moisture and impurities will be removed. Thus, a composite of a 75:25 ratio of cobalt ferrite and nanocellulose fibers was obtained.

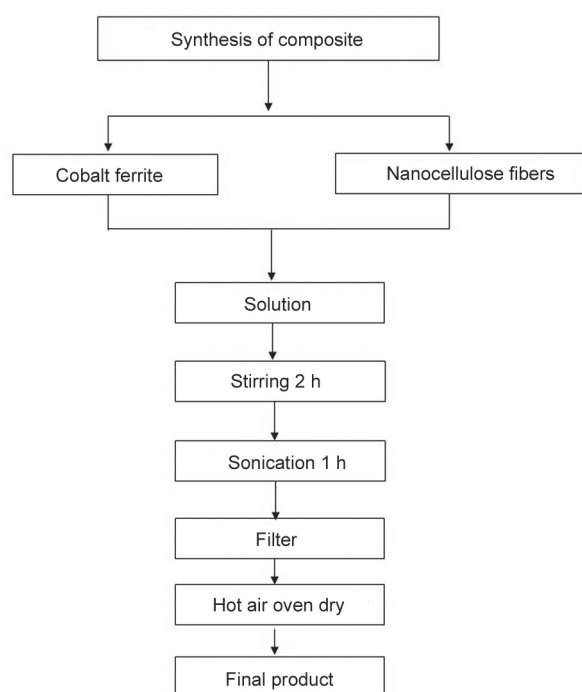


Figure 3. Flow chart for the synthesis of cobalt ferrite-nanocellulose fiber composite.

3. Characterization

X-ray diffraction (XRD, Smart Lab SE) investigated the crystal structure of samples. The diffraction patterns were recorded over a range of 10 to 80°. Fourier-transform infrared spectroscopy (FTIR) spectrums were collected at 400–4000 cm^{-1} wavelength range using Alpha II (80 ATR) with a resolution of 4 cm^{-1} for 16 scans. Scanning electron microscopy (ZEISS EVO 60 scanning electron microscope with Oxford EDAX Detector) was used to characterize the morphology of NCF and cobalt nanoferrite composites

with a high resolution of 3.0 nm (at 30 kV, SE image). Along with SEM, the EDAX studies were also performed for the elemental analysis.

4. Results and discussions

4.1. XRD

The XRD patterns CF, NCF, 50:50, and 75:25 composite are shown in Figure 4. For cobalt ferrite, in the intensity plot, vs. 2θ six peaks are obtained. It has been observed that prominent peaks are observed for 2θ values of 30.11° , 35.33° , 43.16° , 53.39° , 57.08° and 62.44° . The peak with higher intensity is found at 35.33° . The CF phase's peak positions align with JCPDS card No. 22-1086. Bragg's law incorporates the 2θ values of corresponding peaks for evaluating the interplanar spacing. By incorporating full width and half maximum values of different peaks, particle size has been calculated by Scherer's equation (Equation (1)) [22]:

$$D = \frac{0.9\lambda}{\beta \cos \theta} \quad (1)$$

where D is the particle diameter [Å], λ is the wavelength of X-rays used, β is the full width half maximum.

From calculations, the particle size of cobalt ferrite is found to be between 15–28 nm. Interplanar spacing and $(h k l)$ values for various Bragg angles of cobalt ferrite (CF) and NCF were depicted in Table 1 and Table 2.

For the nanocellulose fibers, only two dominant peaks are obtained at 15.2° and 22.4° , the latter being the most intense peak. The broader peak denotes the semi-crystalline nature of nanocellulose fibers, while

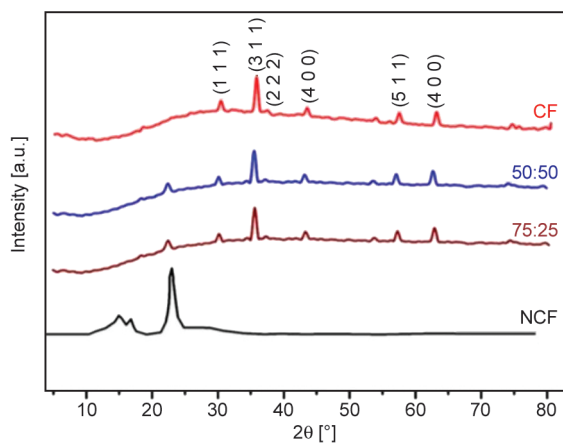


Figure 4. XRD pattern of CF, 50:50, 75:25, and NCF composite.

Table 1. Interplanar spacing values for various Bragg angles of cobalt ferrite (CF).

2θ [°]	$(h k l)$ values	Interplanar spacing [Å]
30.11	(2 2 0)	2.959
35.33	(3 1 1)	2.525
43.16	(4 0 0)	2.092
53.39	(4 2 2)	1.711
57.08	(5 1 1)	1.611
62.44	(4 4 0)	1.480

Table 2. Interplanar spacing values of nanocellulose ferrite (NCF).

2θ [°]	$(h k l)$ values	Interplanar spacing [Å]
15.2	(1 0 0)	2.959
22.4	(0 2 0)	2.525

the sharp, intense peak demonstrated crystallinity [12]. The planes corresponding to the first and second peaks are (1 0 0) and (0 2 0). Nanocellulose fibers size is in 20–30 nm range [21].

For the cobalt ferrite- nanocellulose fibers composite (50:50), peaks are observed at 22.4° , 30.11° , 35.33° , 43.16° , 53.39° , 57.08° , and 62.44° . The peak found at 22.4° confirms the nanocellulose fibers in the composite 50:50. The peak found in both the composites indicates the presence of nanocellulose fiber in both compounds [29]. Similarly, for cobalt ferrite-nanocellulose fibers composite (75:25), peaks are observed at 22.4° , 30.11° , 35.33° , 43.16° , 53.39° , 57.08° and 62.44° . The peak found at 22.4° confirms the nanocellulose fibers in composite 75:25. In both cases, the intensity of the peak in the composite has been diminished compared to that of pure nanocellulose fibers [30]. The peaks obtained at 30.11° , 35.33° , 43.16° , 53.39° , 57.08° and 62.44° are due to the characteristic peak of cobalt ferrite [28]. The lattice spacing calculated for the corresponding peak of composites is the same as that of values obtained for pure material [31]. These values are depicted in the table. There is a reduction in crystallinity with the introduction of nanocellulose fibers. The composite with 25% of nanocellulose fibers exhibited less crystallinity. The aggregation of the iron oxide nanoparticles accounts for the difference in particle and crystalline size [32]. The average crystallite size was 24 and 24.26 nm for the 50:50 and 75:25 composites respectively.

4.2. FTIR

FTIR spectra of CF, NCF, 50:50, and 75:25 composites are shown in Figure 5. For the pure cobalt ferrite, it has been observed that the peak is obtained at 600 cm^{-1} in the fingerprint region confirms that the given sample is a ferrite. This is obtained due to the intrinsic vibration of Fe–O in the tetrahedral position. Some peaks are observed in the region of $3400\text{--}1600\text{ cm}^{-1}$, attributing to the H–O–H bond due to moisture. Thus, it reveals the moisture in the surface of cobalt ferrite. Further, the absence of a peak in the bond region confirms the non-presence of –OH, C=O, C=H, and C–C [33].

Nanocellulose fibers are an organic material consisting of a series of pyranose rings connected by glycosidic linkage. Some of the peaks are due to evidence of an aromatic pyranose ring, which is the base structure of cellulose. Peaks obtained in finger print region are attributed to this pyranose ring, *i.e.*, from 600 to 1500 cm^{-1} . Many peaks are obtained in the bond region ($1500\text{--}4000\text{ cm}^{-1}$). These peaks are observed due to glycosidic linkage among the pyranose ring. Cellulose shows spinel properties due to the sample's crystalline and amorphous nature [34].

Fingerprint region

The peak obtained at 1059 cm^{-1} confirms the Aromatic pyranose ring's presence. Absorbance at this region is due to the C–O–C vibration of the pyranose ring. Peak obtained at 1110 cm^{-1} around due to inter pyranose CH bonding. The absorbance at 1161 cm^{-1} confirms C–C stretching between the carbon atoms in the same pyranose ring. Absorbance is observed in cellulose FTIR due to crystallinity properties in the range 1870 to 880 cm^{-1} . Due to acid hydrolysis

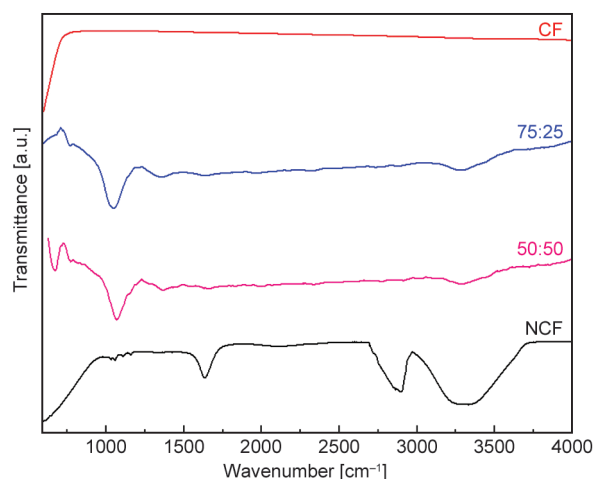


Figure 5. FTIR of CF, 75:25, 50:50, and NCF.

in the pre-treatment process, the material's crystallinity is lost, which can be seen with an absence of a peak at 870 cm^{-1} .

Bond region observations

The broad absorbance is observed in the region from $3300\text{--}3350\text{ cm}^{-1}$ with the highest absorbance at 3329 cm^{-1} ; this is due to the bending of –OH linkage that is present in the aromatic pyranose ring. Sharp absorbance is detected at $2890\text{--}2910\text{ cm}^{-1}$, and higher absorbance is observed at 2902 cm^{-1} . This absorbance is due to the symmetric vibration of CH_2 molecule present in the pyranose ring. Another absorbance at 1635 cm^{-1} which a characteristic feature of TEMPO-oxidised nanocellulose. This absorbance is due to the presence of the carbonyl group. A peak at 1420 cm^{-1} indicates the presence of – CH_2 [34].

For nanocellulose-cobalt ferrite (50:50), significant absorbance are found at 636 , 1049 , 1348 , 1631 , 2917 , and 328 cm^{-1} . From the analysis of the fingerprint region of cobalt ferrite, a strong Fe–O metallic band at 583 cm^{-1} has been observed [33]. This indicates the presence of Fe–O bond in the nanocellulose fibers - cobalt ferrite composite and confirms a strong presence of cobalt ferrite and nanocellulose fibers. Pure nanocellulose fibers do not show any absorbance in the $580\text{--}600\text{ cm}^{-1}$. Similarly, in FTIR of composites 50:50 composites, strong absorbance is observed at 3282 cm^{-1} , confirming the presence of –OH bonds of pyranose rings, thus which are due to the vibration of the intra-molecular O–H–O hydrogen bond. Absorbance is determined in region $2900\text{--}2920\text{ cm}^{-1}$ in the case of nanocellulose; the sharp peak at 2902 cm^{-1} accounts for –CH bonding in the pyranose ring. No such absorbance is obtained in FTIR of cobalt ferrite; thus, the absorbance obtained at 2917 and 2908 cm^{-1} in the case of composite nanocellulose fibers-cobalt ferrite (50:50) is attributed to – CH_2 bond present in the pyranose ring of nanocellulose fiber [19].

Nanocellulose fibers contain cellulose both in crystalline and amorphous form. In nanocellulose fibers, absorbance has been found at 1420 cm^{-1} , accounting for the crystallinity of cellulose. But in the case of both the composites, there is no absorbance at this region, indicating the vanishing of crystallinity of the nanocellulose fibers. In the case of nanocellulose Fibers, the carbonyl group is confirmed by absorbance at 1635 cm^{-1} , a characteristic feature of tempo oxidized nanocellulose fibers. The peak in the same region obtained for nanocellulose fiber-cobalt

ferrite composite (50:50) at 1631 cm^{-1} confirms the presence of carbonyl group in the composite. The absorbance peak obtained at 1049 and 1059 cm^{-1} of cobalt ferrite-nanocellulose fibers (50:50), confirmed the C–O–C bond of the pyranose ring in the given composite [31]. Bond regions of pure cobalt ferrite, nanocellulose fibers, and composites are represented in Table 3.

For the FTIR spectra of nanocellulose fibers-cobalt ferrite (75:25), significant absorbance peaks are identified at $599, 1059, 1347, 1631, 2908, 3282\text{ cm}^{-1}$. From the fingerprint region of cobalt ferrite analysis, the strong Fe–O metallic band at 583 cm^{-1} have been observed. This indicates the presence of Fe–O bond in the nanocellulose fiber-cobalt ferrite composite and hence confirms nanocellulose fibers. The strong absorbance is observed at 3282 cm^{-1} , assuring the presence of –OH bonds of pyranose rings, thus which are due to the vibration of the intra-molecular O–H–O hydrogen bond. Absorbance is determined in region $2900\text{--}2920\text{ cm}^{-1}$ in the case of nanocellulose, the sharp peak at 2902 cm^{-1} accounts for –CH bonding in the pyranose ring. No such absorbance is obtained in FTIR of cobalt ferrite; thus, the absorbance obtained at 2908 cm^{-1} in cobalt ferrite-nanocellulose fiber composite (75:25) confirms that –CH₂ bond present in the pyranose ring of nanocellulose fiber [19]. The carbonyl group in nanocellulose fibers is confirmed by absorbance at 1635 cm^{-1} , a characteristic feature of TEMPO oxidized nanocellulose fibers. The peak in the same region obtained for cobalt ferrite-nanocellulose fiber composite (75:25) at 163 cm^{-1} confirms the presence of the carbonyl group in the composite [35].

In the case of pure nanocellulose fibers, a sharp peak is found at 1059 cm^{-1} due to the vibration of the C–O–C bond. This vibration confirmed the presence of a pyranose ring in nanocellulose fiber. A similar absorbance is obtained at 1049 and 1059 cm^{-1} of cobalt ferrite-nanocellulose fibers (75:25), confirming the C–O–C bond of the pyranose ring in the given composite. From all the above observations, it has seen that there are functional groups are present in the cobalt ferrite by a Fe–O metallic bond. Many organic bonds such as C=O, –CH₂, –O–H, and C–O–C are present in nanocellulose fibers [36].

4.3. SEM studies

SEM of cobalt ferrite has been studied to analyse morphological features like particle size and particle distribution. Figure 6 and Figure 7 represents the SEM image of pure cobalt ferrite and particle distribution in cobalt ferrite. These images are analyzed using ImageJ software. For the image with the magnification of $30\,000\times$ around 100 particles has been observed. This image shows uniform mono-dispersive and cubic structure particles. These particles have been observed in the narrow particle size distribution. The cobalt ferrite calcinated at $600\text{ }^\circ\text{C}$ for 5 h, showing some accumulation [37]. This aggregation is due to the magnetic nature of particles and surface attraction of particles which are accounted for by van der Waal's force. The images captured from the SEM device at $30\,000\times$ magnification show a porous surface in cobalt ferrite.

Using the ImageJ software, particle sizes of many particles have been scaled. Using this tabulated point

Table 3. Bond regions of pure cobalt ferrite, pure nanocellulose fibers, and composites.

Bond region [cm ⁻¹]	Pure CF [cm ⁻¹]	Pure NCF [cm ⁻¹]	NCF-CF composite (50:50) [cm ⁻¹]	CF-NCF composite (75:25) [cm ⁻¹]	Reason for bond formation
580–640	599	–	636	599	Fe–O (metallic bond)
1040–1070	–	1059	1049	1059	C–O (pyranose ring)
1110–1130	–	1110	–	–	C–C (pyranose ring)
1160–1180	–	1161	–	–	C–C (stretching vibration)
1420	–	1420	–	–	–CH ₂
1630–1640	–	1635	1631	1631	C=O, O–H (TEMPO bond)
2900–2920	–	2902	2917	2908	–CH ₂ (symmetric vibrations)
3280–3380	–	3329	3282	3282	–OH (aromatic ring)

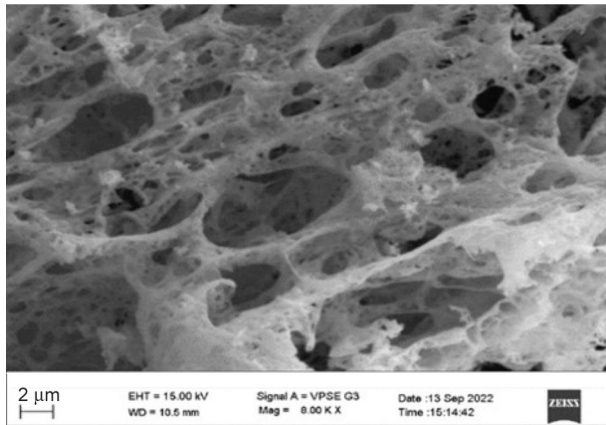


Figure 6. SEM image of pure cobalt ferrite.

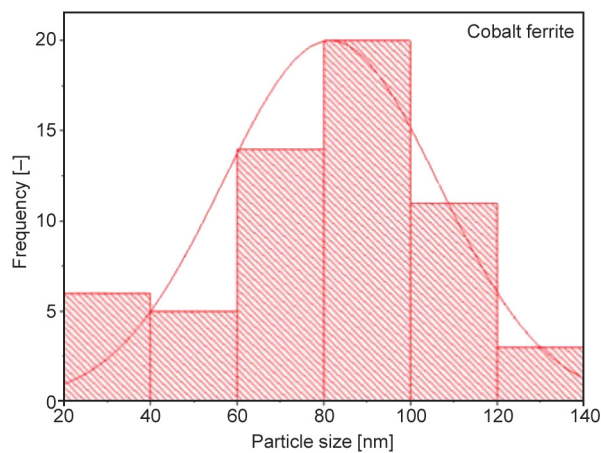


Figure 7. Particle distribution in cobalt ferrite.

histogram has been plotted for analyzing particle size. The histogram shows various particles of different sizes, and its analysis gives the data on average particle size. The average particle size from the histogram plot is formed between 62 to 100 nm. These particle sizes agree with the particle size obtained from XRD [38].

The SEM analysis of nanocellulose fibers confirms the formation of fiber structures arranged in network form (Figure 8). It has been found that these surfaces are rough. The plot histogram gives the average size of nanocellulose was in the 20 to 40 nm range (Figure 9). These values of the diameter of nanocellulose fibers are in agreement with the particle size obtained from XRD analysis.

This validates that nanocellulose fibers with a large surface area have been formed by TEMPO oxidation method. This large surface area maximizes the chemical reactivity of the given surfaces. It has also been found that the nanocellulose ferrite extracted from sugar cane bagasse form process methods that are supportive for adhesion with the other metal oxide nanoparticles [30].

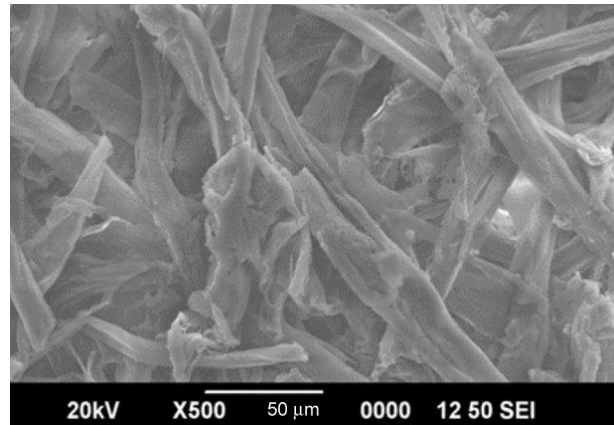


Figure 8. SEM image of nanocellulose fibers.

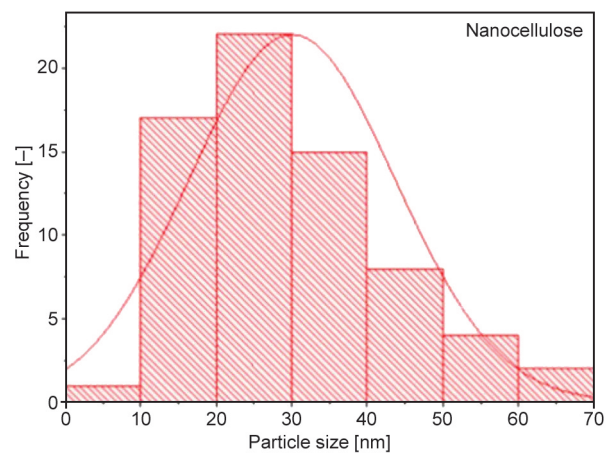


Figure 9. Particle size distribution in nanocellulose fibers.

In SEM images, some little amount of the agglomeration has also been observed for 50:50 composite (Figure 10). The histogram has been plotted for 50:50 composite (Figure 11); the lesser particle size is observed in the composite with a ratio of 50:50, which can be accounted for the more presence of cellulose nanofibers of smaller size [38].

Figure 12 depicts the SEM image of the 75:25 composite. From histogram data, it was found that the particle size in the case of composite with a ratio of 75:25 the particle size lies between 60 to 80 nm (Figure 13). In the case of the composite 75:25, the average particle size is greater. It is due to more percentage of cobalt ferrite with particle size of 60–80 nm. Even in their SEM images, some aggregation has also been observed. The composite shows high porosity and a high surface volume ratio. This property helps produce gas sensors that require high speed and high sensitivity [6].

4.4. Elemental analysis

The analysis of the EDAX spectrum (Figure 14) of cobalt ferrite confirms the elemental composition of

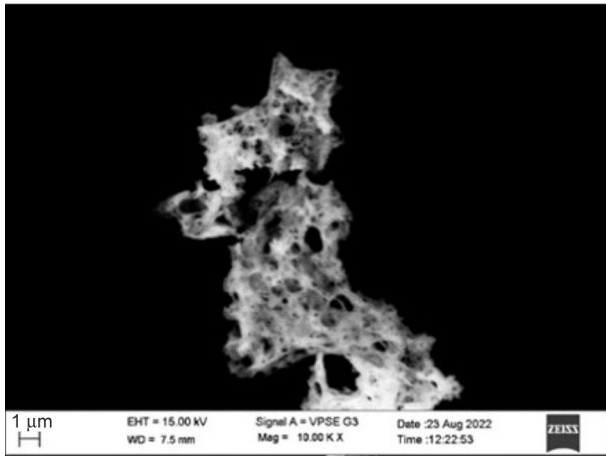


Figure 10. SEM image of 50:50 composite.

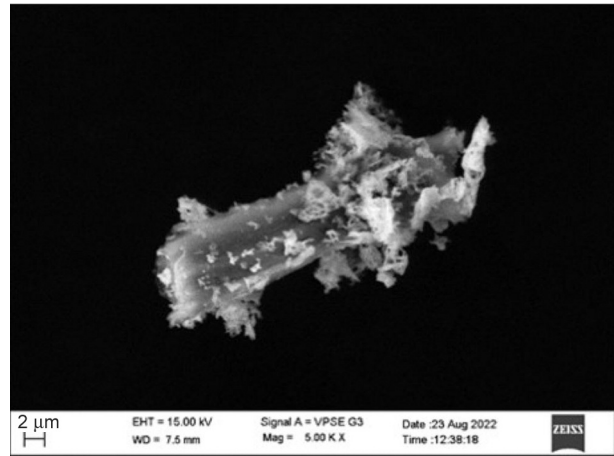


Figure 12. SEM image of 75:25 composite.

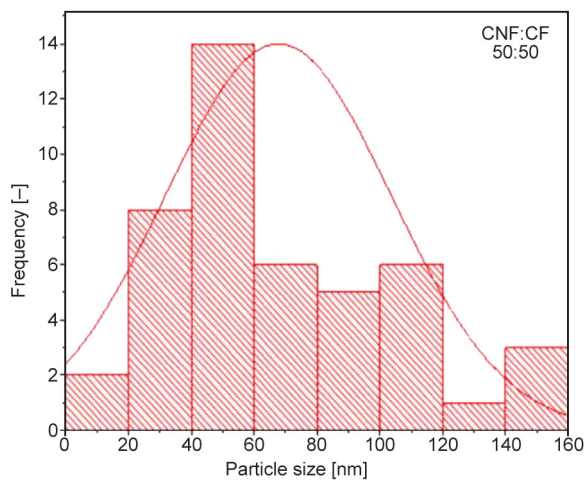


Figure 11. Particle size distribution in cobalt ferrite-nanocellulose fibers composite (50:50).

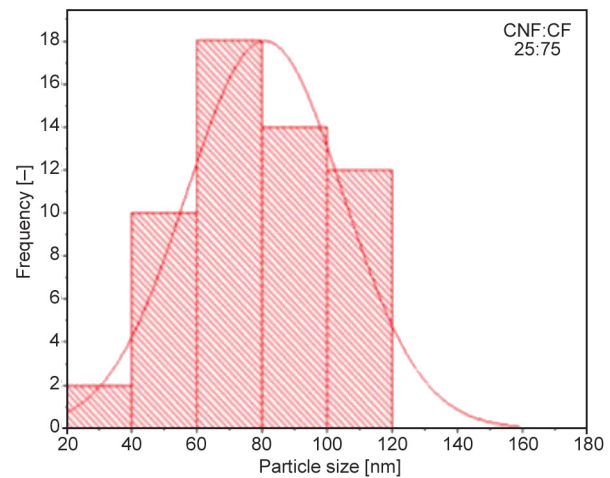


Figure 13. Particle size distribution in cobalt ferrite-nanocellulose fiber composite 75:25.

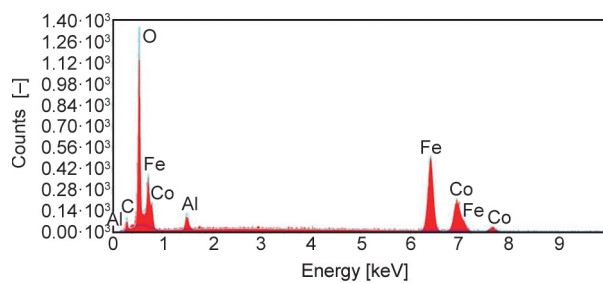


Figure 14. EDAX pattern of cobalt ferrite.

cobalt ferrites. Atomic and molecular composition of cobalt ferrite based on molecular formulae [28]. Table 4 depicts the molar composition and atomic

composition calculated based on molecular formulae of cobalt ferrite.

The EDAX spectra of pure nanocellulose fiber (NCFs) is depicted in Figure 15. Pure nanocellulose fiber is the polymer of the D glucopyranose ring. This structure has a chemical formula $(C_6H_{10}O_5)_n$ where n indicates the number of monomers in the polymer. Usually, it is assumed that there will be a minimum of 200 monomers in the given nanocellulose fiber; this may go up to 30 000. In this analysis, we can confirm the elemental composition of nanocellulose fiber. The EDAX of the nanocellulose fiber shows the presence of carbon and oxygen. The

Table 4. The molar composition and atomic composition are calculated based on molecular formulae of cobalt ferrite.

Element	The ratio of atoms in a mol of $CoFe_2O_4$	The molecular mass of an element [g/mol]	Total contribution to molar mass	Molar composition [%]	Atomic composition [%]
Cobalt	1	58.933	58.933	25.11	14.28
Iron	2	55.845	111.690	47.60	28.56
Oxygen	4	15.999	63.996	27.27	57.16
Total	7	—	234.619	100.00	100.00

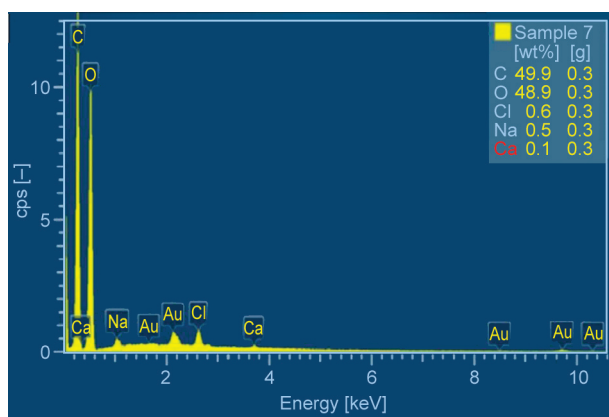


Figure 15. EDAX of nanocellulose fibers.

hydrogen present in the compound is not visible in the energy dispersive spectroscopy since it detects only those elements with mass greater than or equal to carbon. From the analysis, it has been found that 51% of its weight is contributed by oxygen, 48% of its weight is contributed by carbon, whereas 55.97% of its atomic composition is due to carbon, and 44% is due to oxygen present in the glucopyranose ring [28].

The first sample of composite comprised of nanocellulose fibers-cobalt ferrite, and the ratio is 50:50. Here, equal amounts of cobalt ferrite and nanocellulose fiber by weight are taken while synthesizing the composite. Some parts of nanocellulose fiber present in a semi-liquid state contain molecules. The spectrum of EDAX for this composite source is cobalt, iron (Fe), oxygen, and carbon molecules. The presence of iron (Fe) and cobalt (Co) accounts for cobalt ferrite. Table 5 and Table 6 shows the atomic and

Table 5. Atomic and molecular composition of cobalt ferrite obtained from EDAX obtained data.

Element	Weight [%]	Atomic [%]	Error [%]
Carbon	3.8	11.1	18.5
Oxygen	17.7	38.9	8.9
Aluminum	1.9	2.5	13.1
Iron	49.8	31.4	4.2
Cobalt	26.8	16.0	5.8

Table 6. The weight and atomic percentage of EDAX.

Element	Weight (from molecular formulae) [%]	Weight (from EDS) [%]	Atomic (molecular formulae) [%]	Atomic (EDS) [%]
Carbon	–	3.8	–	11.1
Oxygen	27.28	17.7	57.16	38.9
Aluminum	–	1.9	–	2.5
Iron	47.60	49.8	28.56	31.4
Cobalt	25.12	26.8	14.28	16.0

molecular composition of cobalt ferrite obtained from EDAX obtained data and the weight and atomic percentage of EDAX respectively.

The carbon present in the spectrum (Figure 16) results due to the presence of nanocellulose fiber monomer glucopyranose ring. The oxygen present in the spectrum represents both cobalt ferrite and nanocellulose fiber. Most of this oxygen is present in a glycosidic linkage and hydroxyl bonds, as studied in FTIR analysis of nanocellulose fiber. The composition scale shows the presence of carbon which accounts for 8% of composite weight and 21.3% of the total number of atoms in the composite; all the carbon is attributed only to nanocellulose fiber. Oxygen weight is 18.3% by weight and 36.4% by atomic composition; this oxygen results from both nanocellulose fiber and cobalt ferrite. The iron is detected in the spectrum, which comprises 45.9% of the total weight of the composite and 26.2% of the total number of atoms. This iron accounts for the presence of cobalt ferrite from EDAX analysis contribution of cobalt is found to be 26.1% for the total weight and 14.1% for the entire atomic compositions. All these values are in agreement with the compositions that have been utilized in the synthesis step. A slight loss of oxygen is found, which may be attributed to the water molecule’s evaporation in ferrites’ formation. A small amount of aluminum, which accounts for only 1.6%, is found as an impurity. Thus, we can confirm composite formation in the ratio 50:50 [28]. Table 7 represents weight and atomic percentage of cobalt ferrite-nanocellulose fiber composite (50:50).

The EDAX of cobalt ferrite-nanocellulose fibers composite (75:25) is shown in Figure 17. Table 8 represents weight and atomic percentage of cobalt ferrite-nanocellulose fiber composite (75:25). The spectrum of EDAX for this composite is the presence of cobalt, iron (Fe), oxygen, and carbon molecules. The presence of iron (Fe) and cobalt (Co) accounts for cobalt ferrite. The carbon in the spectrum

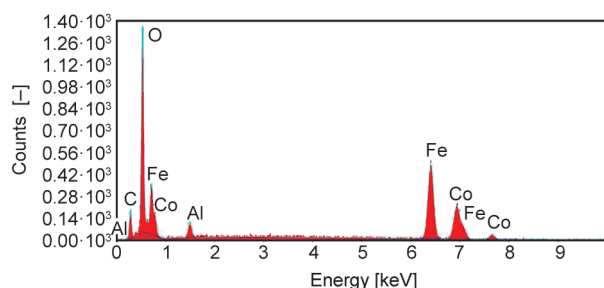


Figure 16. EDAX of cobalt ferrite- nanocellulose fibers composite (50:50).

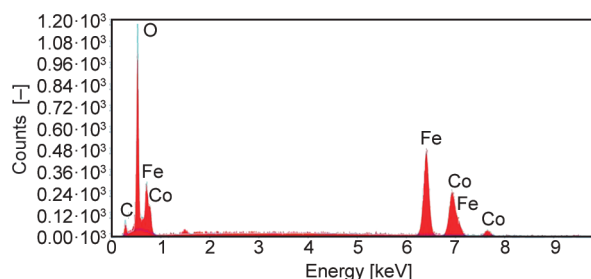


Figure 17. EDAX of cobalt ferrite - nanocellulose fibers composite (75:25).

Table 7. Weight and atomic percentage of cobalt ferrite-nanocellulose fiber composite (50:50).

Element	Weight [%]	Atomic [%]	Error [%]
C K	8.0	21.3	14.3
O K	18.3	36.4	9.2
Al K	1.6	1.9	13.4
Fe K	45.9	26.2	4.2
Co K	26.1	14.1	5.6

Table 8. Weight and atomic percentage of cobalt ferrite-nanocellulose fiber composite (75:25).

Element	Weight [%]	Atomic [%]	Error [%]
C K	3.9	12.0	18.3
O K	15.4	35.6	9.0
Al K	1.7	1.8	13.4
Fe K	48.2	32.0	4.3
Co K	32.5	20.4	5.5

results from the nanocellulose fiber monomer glucopyranose ring. The oxygen present in the spectrum represents both cobalt ferrite and nanocellulose fiber. The composition scale shows the presence of carbon which accounts for 39% of the weight of the composite and 12% of the total number of atoms in the composite; all the carbon is attributed only to nanocellulose fiber. Oxygen weight is 54% by weight and 35.6% by atomic composition. This oxygen is a result of both nanocellulose fiber and cobalt ferrite. The iron has been detected in the spectrum, which compresses 48.2% of the total weight of the composite and 32% of the total number of atoms. The iron accounts for the presence of cobalt ferrite from EDAX analysis contribution of cobalt is found to be 35.5% for the total weight and 20% for the complete atomic compositions [39].

All these values are in agreement with the compositions. A slight loss of oxygen is found, which may be accounted for by the evaporation of water molecules in the formation of Ferrites. No other impurities are detected.

5. Conclusions

Using cellulose nanofibers as a template, a straightforward sol-gel approach was utilized to create magnetic cobalt nanoparticles with a limited size distribution. The fibrous network structured cellulose Nanofiber is synthesized by following the TEMPO-oxidation method, the crude cellulose was extracted

from sugarcane bagasse, and the composite of this substance was synthesized by treating both cobalt ferrite and nanocellulose once in the ratio of 50:50 and 75:25 respectively. The magnetic nanocellulose samples containing different concentrations of cellulose nanofibers were further characterized by XRD and FTIR to understand the mechanism of nanoparticle formation on the surfaces of cellulose nanofibers. For cobalt ferrite, maximum intensity is obtained at 35.33° , confirming its formation and a particle size between 15–28 nm. XRD analysis of pure nanocellulose fibers showed peak intensity at 22.40° with Scherrer's formula, and the particle size was 7.86–20 nm. The FTIR analysis confirms the formation of composites by detecting absorbance at $580\text{--}640\text{ cm}^{-1}$ which indicates the presence of Fe–O metallic bond, and $1040\text{--}1070\text{ cm}^{-1}$ which indicates pyranose. This proves the existence of cobalt ferrite and nanocellulose fibers in the composites. The SEM analysis of the composites reveals the formation of nanocellulose fibers-cobalt ferrites composites with particles showing less agglomeration. Composite with a higher concentration of nanocellulose fibers shows lesser particle size, this may be accounted for the smaller size of nanocellulose fibers, attachment of nano cellulose nanofibers over the surface of porous cobalt ferrite is clearly found in SEM images. Cobalt ferrite, nanocellulose fibers, and composites are highly valued for their unique morphological and structural characteristics.

References

- [1] Chae D. W., Kim B. C.: Characterization on polystyrene/zinc oxide nanocomposites prepared from solution mixing. *Polymers for Advanced Technologies*, **16**, 846–850 (2005).
<https://doi.org/10.1002/pat.673>
- [2] Cao M-S., Yang J., Song W-L., Zhang D-Q., Wen B., Jin H-B., Hou Z-L., Yuan J.: Ferroferric oxide/multiwalled carbon nanotube vs. polyaniline/ferroferric oxide/multiwalled carbon nanotube multiheterostructures for highly effective microwave absorption. *ACS Applied Material Interfaces*, **4**, 6949–6956 (2012).
<https://doi.org/10.1021/am3021069>
- [3] Barreto A. C. H., Santiago V. R., Mazzetto S. E., Denardin J. C., Lavin R., Mele G., Ribeiro M. E. N. P., Vieira I. G. P., Gonçalves T., Ricardo N. M. P. S., Fechine P. B. A.: Magnetic nanoparticles for a new drug delivery system to control quercetin releasing for cancer chemotherapy. *Journal of Nanoparticle Research*, **13**, 6545–6553 (2011).
<https://doi.org/10.1007/s11051-011-0559-9>
- [4] Hao R., Xing R., Xu Z., Hou Y., Gao S., Sun S.: Synthesis, functionalization, and biomedical applications of multifunctional magnetic nanoparticles. *Advanced Materials*, **22**, 2729–2742 (2010).
<https://doi.org/10.1002/adma.201000260>
- [5] Lee N., Hyeon T.: Designed synthesis of uniformly sized iron oxide nanoparticles for efficient magnetic resonance imaging contrast agents. *Chemical Society Reviews*, **41**, 2575–2589 (2012).
<https://doi.org/10.1039/C1CS15248C>
- [6] Tian C., Fu S., Lucia L. A.: Magnetic $\text{Cu}_{0.5}\text{Co}_{0.5}\text{Fe}_2\text{O}_4$ ferrite nanoparticles immobilized *in situ* on the surfaces of cellulose nanocrystals. *Cellulose*, **22**, 2571–2587 (2015).
<https://doi.org/10.1007/s10570-015-0658-3>
- [7] Lee C-M., Jeong H-J., Lim S-T., Sohn M-H., Kim D-W.: Synthesis of iron oxide nanoparticles with control over shape using imidazolium-based ionic liquids. *ACS Applied Material Interfaces*, **2**, 756–759 (2010).
<https://doi.org/10.1021/am900769x>
- [8] Laurent S., Forge D., Port M., Roch A., Robic C., Vander Elst L., Muller R. N.: Magnetic iron oxide nanoparticles: Synthesis, stabilization, vectorization, physicochemical characterizations, and biological applications. *Chemical Reviews*, **108**, 2064–2110 (2008).
<https://doi.org/10.1021/cr068445e>
- [9] Lüders U., Barthélémy A., Bibes M., Bouzehouane K., Fusil S., Jacquet E., Contour J. P., Bobo J. F., Fontcuberta J., Fert A.: NiFe_2O_4 : A versatile spinel material brings new opportunities for spintronics. *Advanced Materials*, **18**, 1733–1736 (2006).
<https://doi.org/10.1002/adma.200500972>
- [10] Baig R. B. N., Nadagouda M. N., Varma R. S.: Carbon-coated magnetic palladium: Applications in partial oxidation of alcohols and coupling reactions. *Green Chemistry*, **16**, 4333 (2014).
<https://doi.org/10.1039/C4GC00748D>
- [11] Rezlescu N., Rezlescu E., Sava C. L., Tudorache F., Popa P. D.: Effects of some ionic substitutions on sintering, structure and humidity sensitivity of MgCu ferrite. *Physica Status Solidi (a)*, **201**, 17–25 (2004).
<https://doi.org/10.1002/pssa.200306713>
- [12] Sivakumar M., Takami T., Ikuta H., Towata A., Yasui K., Tuziuti T., Kozuka T., Bhattacharya D., Iida Y.: Fabrication of zinc ferrite nanocrystals by sonochemical emulsification and evaporation Observation of magnetization and its relaxation at low temperature. *Journal of Physical Chemistry B*, **110**, 15234–15243 (2006).
<https://doi.org/10.1021/jp055024c>
- [13] Moon R. J., Martini A., Nairn J., Simonsen J., Youngblood J.: Cellulose nanomaterials review: Structure, properties and nanocomposites. *Chemical Society Reviews*, **40**, 3941–3994 (2011).
<https://doi.org/10.1039/c0cs00108b>
- [14] Walther A., Timonen J. V. I., Díez I., Laukkanen A., Ikkala O.: Multifunctional high-performance biofibers based on wet-extrusion of renewable native cellulose nanofibrils. *Advanced Materials*, **23**, 2924–2928 (2011).
<https://doi.org/10.1002/adma.201100580>
- [15] Kępa K., Chaléat C. M., Amiralian N., Batchelor W., Grøndahl L., Martin D. J.: Evaluation of properties and specific energy consumption of spinifex-derived lignocellulose fibers produced using different mechanical processes. *Cellulose*, **7**, 6555–6569 (2019).
<https://doi.org/10.1007/s10570-019-02567-x>
- [16] Pennells J., Godwin I. D., Amiralian N., Martin D. J.: Trends in the production of cellulose nanofibers from non-wood sources. *Cellulose*, **27**, 575–593 (2020).
<https://doi.org/10.1007/s10570-019-02828-9>
- [17] Bourrioux S., Wang L. P., Rousseau Y., Simon P., Habert A., Leconte Y., Sougrati M. T., Stievano L., Monconduit L., Xu Z. J., Srinivasan M., Pasturel A.: Evaluation of electrochemical performances of $\text{ZnFe}_2\text{O}_4/\gamma\text{-Fe}_2\text{O}_3$ nanoparticles prepared by laser pyrolysis. *New Journal of Chemistry*, **41**, 9236–9243 (2017).
<https://doi.org/10.1039/C7NJ00735C>
- [18] Pirkkalainen K., Leppänen K., Vainio U., Webb M. A., Elbra T., Kohout T., Nykänen A., Ruokolainen J., Kotelnikova N., Serimaa R.: Nanocomposites of magnetic cobalt nanoparticles and cellulose. *The European Physical Journal D*, **49**, 333–342 (2008).
<https://doi.org/10.1140/epjd/e2008-00180-5>
- [19] Amiralian N., Mustapic M., Hossain M. S. A., Wang C., Konarova M., Tang J., Na J., Khan A., Rowan A.: Magnetic nanocellulose: A potential material for removal of dye from water. *Journal of Hazardous Materials*, **394**, 122571 (2020).
<https://doi.org/10.1016/j.jhazmat.2020.122571>
- [20] Oprea M., Panaitescu D. M.: Nanocellulose hybrids with metal oxides nanoparticles for biomedical applications. *Molecules*, **25**, 4045 (2020).
<https://doi.org/10.3390/molecules25184045>

- [21] Korotcenkov G.: Electrospun metal oxide nanofibers and their conductometric gas sensor application. Part 1: Nanofibers and features of their forming. *Nanomaterials*, **11**, 1544 (2021).
<https://doi.org/10.3390/nano11061544>
- [22] Toksha B. G., Shirsath S. E., Patange S. M., Jadhav K. M.: Structural investigations and magnetic properties of cobalt ferrite nanoparticles prepared by sol-gel auto combustion method. *Solid State Communications*, **147**, 479–483 (2008).
<https://doi.org/10.1016/j.ssc.2008.06.040>
- [23] Phanthong P., Reubroycharoen P., Hao X., Xu G., Abudula A., Guan G.: Nanocellulose: Extraction and application. *Carbon Resources Conversion*, **1**, 32–43 (2018).
<https://doi.org/10.1016/j.crcon.2018.05.004>
- [24] Isaza L. G., Mortha G., Marlin N., Molton F., Duboc C.: ClO₂-mediated oxidation of the TEMPO radical: Fundamental considerations of the catalytic system for the oxidation of cellulose fibers. *Molecules*, **28**, 6631 (2023).
<https://doi.org/10.3390/molecules28186631>
- [25] Jagadesh P., Ramachandramurthy A., Murugesan R.: Evaluation of mechanical properties of sugar cane bagasse ash concrete. *Construction and Building Materials*, **176**, 608–617 (2018).
<https://doi.org/10.1016/j.conbuildmat.2018.05.037>
- [26] Yu H., Qin Z., Liang B., Liu N., Zhou Z., Chen L.: Facile extraction of thermally stable cellulose nanocrystals with a high yield of 93% through hydrochloric acid-hydrolysis under hydrothermal conditions. *Journal of Materials Chemistry A*, **1**, 3938 (2013).
<https://doi.org/10.1039/c3ta01150j>
- [27] Bragđ P. L., van Bekkum H., Besemer A. C.: TEMPO-mediated oxidation of polysaccharides: Survey of methods and applications. *Topics in Catalysis*, **27**, 49–66 (2004).
<https://doi.org/10.1023/B:TOCA.0000013540.69309.46>
- [28] Rahimi Kord Sofla M., Brown R. J., Tsuzuki T., Rainey T. J.: A comparison of cellulose nanocrystals and cellulose nanofibres extracted from bagasse using acid and ball milling methods. *Advances in Natural Sciences: Nanoscience and Nanotechnology*, **7**, 035004 (2016).
<https://doi.org/10.1088/2043-6262/7/3/035004>
- [29] Wu Y., Xu L., Shi J., Cui J., Han S., Xia C., Gan L.: Cobalt ferrite/cellulose membrane inserted catalytic syringe filter for facile *in-situ* filtration/degradation of emerging organic pollutants in water *via* activating peroxymonosulfate. *Materials & Design*, **220**, 110817 (2022).
<https://doi.org/10.1016/j.matdes.2022.110817>
- [30] Srasri K., Thongroj M., Chaijiraaree P., Thiangtham S., Manuspiya H., Pisitsak P., Ummartyotin S.: Recovery potential of cellulose fiber from newspaper waste: An approach on magnetic cellulose aerogel for dye adsorption material. *International Journal of Biological Macromolecules*, **119**, 662–668 (2018).
<https://doi.org/10.1016/j.ijbiomac.2018.07.123>
- [31] Menchaca-Nal S., Londoño-Calderón C. L., Cerrutti P., Foresti M. L., Pampillo L., Bilovol V., Candal R., Martínez-García R.: Facile synthesis of cobalt ferrite nanotubes using bacterial nanocellulose as template. *Carbohydrate Polymers*, **137**, 726–731 (2016).
<https://doi.org/10.1016/j.carbpol.2015.10.068>
- [32] Rusmirović J. D., Ivanović J. Z., Pavlović V. B., Rakić V. M., Rančić M. P., Djokić V., Marinković A. D.: Novel modified nanocellulose applicable as reinforcement in high-performance nanocomposites. *Carbohydrate Polymers*, **164**, 64–74 (2017).
<https://doi.org/10.1016/j.carbpol.2017.01.086>
- [33] Connes J., Connes P.: Near-infrared planetary spectra by fourier spectroscopy. I. Instruments and results. *Journal of the Optical Society of America*, **56**, 896 (1966).
<https://doi.org/10.1364/JOSA.56.000896>
- [34] Oh S. Y., Yoo D. I., Shin Y., Seo G.: FTIR analysis of cellulose treated with sodium hydroxide and carbon dioxide. *Carbohydrate Research*, **340**, 417–428 (2005).
<https://doi.org/10.1016/j.carres.2004.11.027>
- [35] Soni B., Hassan E. B., Mahmoud B.: Chemical isolation and characterization of different cellulose nanofibers from cotton stalks. *Carbohydrate Polymers*, **134**, 581–589 (2015).
<https://doi.org/10.1016/j.carbpol.2015.08.031>
- [36] Nelson M. L., O'Connor R. T.: Relation of certain infrared bands to cellulose crystallinity and crystal latticed type. Part I. Spectra of lattice types I, II, III and of amorphous cellulose. *Journal of Applied Polymer Science*, **8**, 1311–1324 (1964).
<https://doi.org/10.1002/app.1964.070080322>
- [37] Londoño-Calderón C. L., Londoño-Calderón A., Menchaca-Nal S., Salazar-Henao N. A., Rosales-Rivera A., Pampillo L. G., Martínez-García R.: Magnetic properties of cobalt ferrite octahedrons obtained from calcination of granular nanotubes growing on bacterial nanocellulose. *Journal of Magnetism and Magnetic Materials*, **495**, 165899 (2020).
<https://doi.org/10.1016/j.jmmm.2019.165899>
- [38] Prusty K., Sahu D., Swain S. K.: Nanocellulose as a template for the production of advanced nanostructured material. in ‘Cellulose-reinforced nanofibre composites’ (eds.: Jawaid M., Boufi S., Abdul Khalil H. P. S.) Woodhead, Cambridge, 427–454 (2017).
<https://doi.org/10.1016/B978-0-08-100957-4.00019-X>
- [39] Valencia L., Kumar S., Nomena E. M., Salazar-Alvarez G., Mathew A. P.: *In-situ* growth of metal oxide nanoparticles on cellulose nanofibrils for dye removal and antimicrobial applications. *ACS Applied Nano Materials*, **3**, 7172–7181 (2020).
<https://doi.org/10.1021/acsanm.0c01511>